Interlayers Engineering for Flexible Large-Area Planar Perovskite Solar Cells

Jia Li, [1] *Guifang Han,* [1] *Kurt Vergeer,* [1] *Herlina Arianita Dewi,* [1] *Hao Wang,* [1] *Subodh Mhaisalkar,* [1, 2] *Annalisa Bruno,*[1]* *Nripan Mathews* [1, 2]

[1] *Energy Research Institute @ Nanyang Technological University (ERI@N)*

Research Techno Plaza, X-Frontier Block, Level 5, 50 Nanyang Drive 637553, Singapore

[2] *School of Materials Science and Engineering, Nanyang Technological University*

50 Nanyang Avenue 639798, Singapore

Corresponding Author

* Email: Annalisa@ntu.edu.sg

Key Words:

Flexible, Perovskite, Solar Cells, Low Temperature TiO_2, Guanidinium Iodide Passivation

Abstract

Hybrid metal halide perovskite solar cells (PSCs) have consistently demonstrated high power conversion efficiency (PCE), although the best performing PSCs mostly employ high-temperature (500 ^{o}C) processed compact and mesoporous TiO_2. Instead, low-temperature processed PSCs are desirable for implementation on flexible substrates and tandem solar cells. Here, we present a new method to achieve high efficiency flexible planar PSCs based on a low-temperature processed nonaqueous sol-gel route synthesized TiO_2 and a guanidinium iodide (GuaI) salt passivation treatment of the perovskite film. We fabricate both rigid and flexible triple-cation perovskite ($Cs_{0.05}$ $(MA_{0.17}FA_{0.83})_{0.95}Pb(I_{0.85}Br_{0.15})_3$, Eg ~1.58 eV) PSCs, achieving PCEs of 19.8% and 17.0% on glass and polyethylene naphtholate, (PEN) substrates respectively. At the same time, rigid and flexible high-bandgap double cation ($FA_{0.85}Cs_{0.15}Pb(I_{0.7}Br_{0.3})_3$, Eg ~1.72 eV) PSCs reached a PCE of 18.0 % and of 15.8%. Moreover, large area (1cm^2) ~1.58 eV and ~1.72 eV-PSCs achieved PCEs of 18.2% and 16.7% PCE on glass substrates and of 16.2% and 13.9% on PEN substrates demonstrating the high uniformity of all the solar cell layers.

\

Introduction

Organic-inorganic metal halide perovskite made a real breakthrough in the photovoltaic community due to their unique properties as high absorption coefficient [1], long carrier diffusion length [2], tunable bandgap [3] and easy processability [4]. Perovskite solar cells (PSCs) have shown a tremendous increase of their power conversion efficiency (PCE) from 3.81% [5] up to over 23% [6-8]. The possibility of all low temperature process for PSCs make them ideal choice to fabricate flexible PSCs which are desirable in many applications as large area, customizable, portable and wearable devices. With the widespread effort, flexible PSCs have reached PCE of over 18.4% [9,10] from the firstly reported 2.6% [11]. Different architecture in inverted [12], planar [13] and mesoporous [14] based on modified low-temperature processed electron and hole transport layers (ETL and HTL) have been explored previously. In p-i-n architectures, the perovskite active layer is usually sandwiched between low-temperature processed materials (*i.e.:* PEDOT: PSS and PCBM, NiO_x and ZnO), yielding PCEs from 4 up to >18% [15-20]. Low-temperature processed compact and mesoporous layers such as ZnO [11,21], $ZnSnO_4$ [22], TiO_2 [23], Nb_2O_5 [9] and SnO_2 [24-29] were also studied in mesoporous and planar flexible PSCs. TiO_2 is one of the widely used n-type material for rigid and flexible PSCs. Low-temperature TiO_2 deposition techniques such as sputtering, atomic layer deposition (ALD), e-beam induced evaporation and nanoparticles spin-coating have been implemented in PSCs [30-37]. Mali *et al.* [30] used RF magnetron sputtering to fabricate a TiO_2 compact layer in flexible planar PSCs achieving PCE of 15.07% and 15.88%, respectively. Di Giacomo *et al*. [31] fabricated flexible mesoporous PSCs reaching a PCE of 8.4% employing a compact ALD-deposited TiO_2 layer UV-treated TiO_2 nanoparticles as mesoporous scaffold. Instead, Zardetto et al. [32] adopted plasma-assisted ALD to prepare the compact TiO_2 layer in the flexible planar PSCs reaching a PCE of 9.2%. Flexible PSCs based on e-beam evaporated TiO_2 were also demonstrated with efficiencies from 12.3% to 13.5% [33,34]. Jeong et al. [35] developed a solution processed Nd-doped TiO_2 compact layer below 50 ^oC for flexible PSCs reaching 16.01% efficiency. Zhou et al. [36] used solution processed TiO_2 nanoparticles achieving the record PCE of 16.36%. It is worth to note that most of the previously reported flexible PSCs are based on 1.55-1.6 eV bandgap perovskites while it is crucial to develop higher bandgap (*i.e.*:1.70-1.8 eV) [38, 39] based solar cells in a low-temperature process for the implementation of flexible tandem. Previously Jiang et al. [40] reported flexible

high bandgap PSCs, (based on fully inorganic perovskite, $CsPbI_2Br$, with E_g ~1.82 eV) and demonstrating an efficiency of 11.73% while Axel et al reported flexible perovskite/perovskite tandem solar cell, reaching a recording efficiency of 21.3% [41].

In this work, we implemented low temperature processed rigid and flexible PSCs based on both triple cation perovskite, $Cs_{0.05}(MA_{0.17}FA_{0.83})_{0.95}Pb(I_{0.85}Br_{0.15})_3$, with ~1.58 eV bandgap and on double cation perovskite, $Cs_{0.15}FA_{0.85}Pb(I_{0.7}Br_{0.3})_3$ with ~1.72 eV bandgap. We developed a new low-temperature method for TiO_2 thin film based on the modification of the TiO_2 nanoparticles synthesis presented in previous works from Tan et al. [42] and Wojciechowski et al. [43]. The highly uniform TiO_2 films have been implemented as electron transport layer (ETL) in n-i-p planar PSCs both on glass and polyethylene naphtholate, PEN substrates. Moreover, the triple and double cation perovskite films were passivated using guanidinium iodide (GuaI) salt to improve their film quality and reduce their recombination losses, in a different way respect to previous work [44-49], where different guanidinium based salts were instead used as additive in perovskite precursor solutions. The champion GuaI-treated ~1.58 eV PSCs demonstrated PCEs of 19.8% on glass and 17.0% on PEN substrates while the champion GuaI-treated 1.72 eV-PSCs achieved efficiency of 18.0% and 15.8%, on glass and PEN respectively. At the same time, rigid large area (1 cm^2) 1.58 eV and 1.72 eV-PSCs achieved significant PCE of 18.2 % achieved PCE of 16.7 % with good reproducibility. While the first flexible large area of 1 cm^2 1.58 eV and 1.72 eV PSCs showed PCE of 16.2% and 13.9% on PEN substrates, respectively

Results

We adopted a low-temperature nonaqueous sol-gel route to synthesis TiO_2 nanoparticles [42, 43, 50]. In 2014 Wojciechowski et al. [43] showed that the low-temperature synthetized TiO_2 nanoparticles can be dispersed in ethanol and stabilized with titanium diisopropoxide bis(acetylacetonate) (TiAcAc). Similarly, in 2017 Tan et al. [42] showed that TiO_2 nanoparticles can also be stabilized in a mixture of chloroform and methanol solvents where Cl^- acts as ligand on the TiO_2 colloidal surface. The main advantage is that the Cl^- ligand, shorter than $AcAc^-$, can lead to improved charge mobility in the material. Combining their findings, we choose to synthetize TiO_2 nanoparticles, disperse them in ethanol and to use extra $TiCl_4$ to passivate TiO_2 nanoparticles. Indeed, the $TiCl_4$ excess induce Cl^- to act as a ligand similarly to the process induced by the presence of chloroform/methanol mixed solvents [42], with the main advantage of

using ethanol, which is a safe and environmentally friendly solvent. The low-temperature TiO_2 synthesis process has been schematized in 5 steps in **Figure 1a**. (i) TiO_2 colloids were prepared by mixing $TiCl_4$ with ethanol and benzyl alcohol at 70 ^oC for 12 h. (ii) Diethyl ether was added to the solution which was then centrifuged to separate TiO_2 nanoparticles (iii) The TiO_2 nanoparticles collected were then dispersed in ethanol and $TiCl_4$ was added in as stabilizer. (iv) TiO_2 thin films were spin coated by TiO_2 nanoparticles suspension. (v) TiO_2 thin films were annealed at 150 ^oC. The compact TiO_2 layers were optimized by varying $TiCl_4$ addition amount (step iii in **Figure 1a**). X-ray diffraction (XRD) patterns of the as-synthesized (0 M $TiCl_4$) and $TiCl_4$ passivated (50 mM $TiCl_4$) TiO_2 nanoparticles show that for both films the diffraction peaks are well consistent with lattice planes of the TiO_2 anatase, **Figure 1b**. [51] SEM images also show improved TiO_2 film quality with $TiCl_4$ addition, **Figure 1c** and **1d**. Indeed, the as-synthesized film presents large aggregates and pinholes highlighted by the green circles in **Figure 1c**. Instead, $TiCl_4$ passivated (50 mM $TiCl_4$) TiO_2 films show a smoother morphology and absence of pinholes, **Figure 1d**. Surface sensitive X-ray photoelectron spectroscopy (XPS) was employed to investigate the surface composition and chemical state of TiO_2 and $TiCl_4$ passivated (50 mM $TiCl_4$) TiO_2 films, **Figure S1**. The main Ti $2p_{3/2}$ peak at 459.1 eV (**Figure S1b**) and O 1s peak at 530.6 eV (**Figure S1c**) for both films prove the formation of TiO_2. The existence of Cl 2p peaks (Cl $2p_{3/2}$ at 198.9 eV and Cl $2p_{1/2}$ at 200.5 eV) in both films prove that the additional $TiCl_4$ retained Cl ligand on TiO_2 surface well, **Figure S1d**. Planar PSCs, based double cation perovskite ($Cs_{0.15}FA_{0.85}Pb(I_{0.7}Br_{0.3})_3$, E_g ~1.72 eV), employing TiO_2 films as electron transport layer were optimized by varying $TiCl_4$ concentrations, **Figure S2**, and the film thickness, **Figure S3 and Figure S4**. In planar architectures, the charge transport between ETL and perovskite can be improved by introducing a PCBM layer at their interface [52, 53], although the light transmittance can be reduced and ETL wettability can also be affected. [54] In our case, the total transmittance only slightly decreased from 78.4%, 76.2%, with PCBM addition, **Figure S5a** and consistently the perovskite absorption spectra, **Figure S5b**. Steady-state and time resolved photoluminescence (TRPL) confirmed an increased quenching with a PCBM layer addition, **Figure S5c** and **Figure S5d**, consistently with a more efficient charge transfer between perovskite and the ETL. [55]

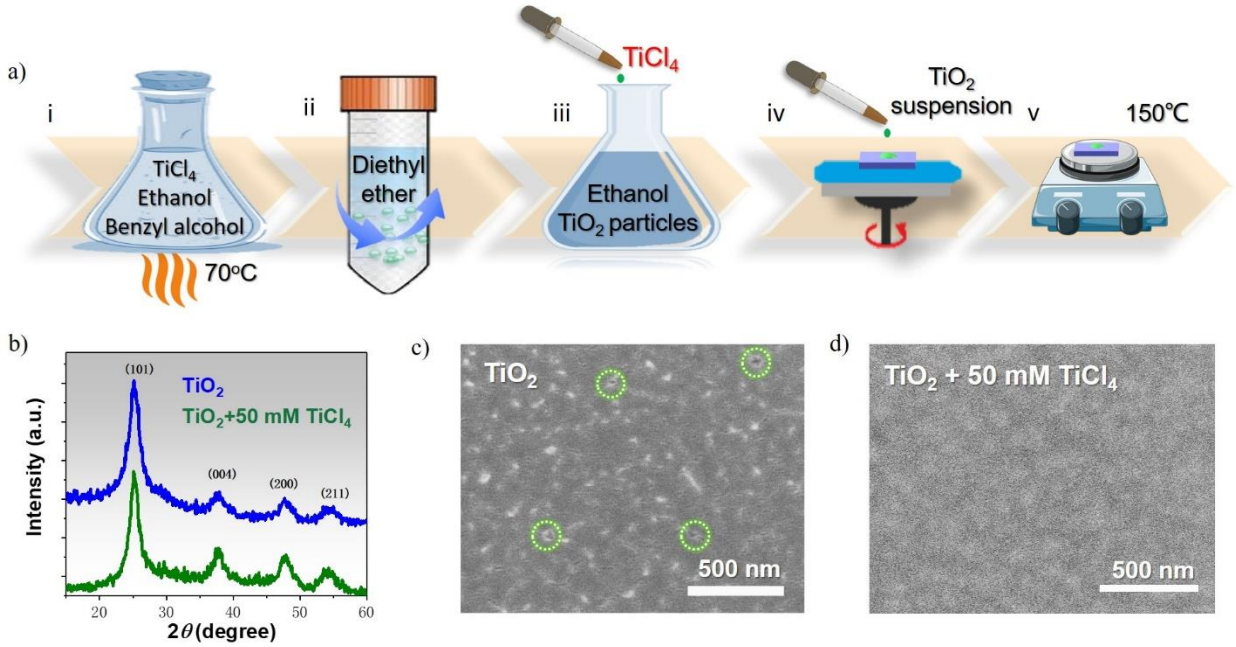

Figure 1. Low-temperature TiO_2 thin films preparation and characterization. a) Schematic process flow overview of low-temperatureTiO_2 films preparation process (i) TiO_2 colloids synthesis (ii) TiO_2 colloids separation and collection by centrifugation (iii) TiO_2 nanoparticles dispersion in ethanol with $TiCl_4$ addition. (iv) TiO_2 thin films spin-coating and (v) annealing at 150 °C for 1 hour. b) XRD spectra of pure TiO_2 and $TiCl_4$-terated TiO_2 films, c) SEM images of pure TiO_2 thin film and d) with 50 mM $TiCl_4$ addition.

PSCs architecture is reported in **Figure 2a** (Glass/FTO/TiO_2/PCBM/1.58 eV &1.72 eV perovskite /Spiro-OMeTAD/Au**)** and the cross-section SEM image, **Figure 2b,** shows the thicknesses of all the layers: TiO_2 ~45 nm, PCBM ~10 nm, perovskite ~500 nm, Spiro-OMeTAD ~150 nm and gold electrode ~100 nm. After the ETL optimization, to further boost the PSC efficiency we implemented a new passivation strategy. Both ~1.58 eV and ~1.72 eV (from here after just indicated as 1.58 and 1.72 eV for simplicity) perovskite films were treated with GuaI salt as passivation agent. Previous works [40-45] employed guanidinium-based salts as additive in the precursor solutions of methylammonium lead iodine ($MAPbI_3$) and in mix cations perovskites (including Cs and MA and Formamidinium) showing that the large guanidinium cation can passivate the under-coordinated iodine species at grain boundaries through their hydrogen bonding capability and so reducing the iodide vacancies, leading to an effective clampdown of the charge recombination in perovskite film and inducing a significantly improvement of the final device stability. Here, for the first time we demonstrate that GuaI effectively works also as passivation agent and not as additive in the precursor solution with the

main advantage that can be used with different optimized perovskite compositions. The GuaI treatment significantly improves the film quality and device performances for both triple (1.58 eV) and double cation (1.72 eV) perovskite, confirming the versatility and generality of the passivation strategy. Details of the preparation and optimization procedure are reported in the Experimental Section and in **Figure S6**. The GuaI-treated $Cs_{0.15}FA_{0.85}Pb(I_{0.7}Br_{0.3})_3$ perovskite films show larger crystal size compared with the untreated films, **Figure S7.** The larger crystals lead to reduced boundary defects concentration and a reduced non-radiative charge recombination as also suggested by the higher steady state photoluminescence (PL) intensity, **Figure S8a** and the longer PL lifetime of the GuaI-treated films, **Figure S8b**. Moreover, in terms of devices, the champion GuaI-treated 1.58 eV PSCs reaches a PCE of 19.8%, while the untreated champion PSC shows a record efficiency of 19.4%, **Figure 2c** and **Table 1**. In a similar way, the champion GuaI-treated 1.72 eV PSC showed PCE of 18.0%, with a 10% relative improvement as compared to the untreated champion 1.72 eV PSC which reached a PCE of 17.1%, **Figure 2d** and **Table 1**. Consistently for both perovskites the GuaI passivation treatment helps to significantly increase the V_{oc} and the fill factor in agreement with the presence of larger grains and reduced charge recombination, **Figure S9 and Figure S10**. Instead, the IPCE spectra of PSCs before and after passivation similarly reached values above 90% for both 1.58 eV and 1.72 eV PSCs, and show unchanged values of the integrated current in agreement with the measured J_{sc}, **Figure S11**. The PSCs were also investigated in the low intensity illumination regime. The GuaI-treated and untreated 1.72 eV PSCs V_{oc} trend as function the light intensity, **Figure 2e**, show respectively a slop of $1.31K_BT/q$ and $1.80\ K_BT/q$, where K_B is the Boltzmann constant, T is temperature and q is the electric charge. The GuaI-treated PSCs smaller slope indicates that the charge recombination in perovskite layer was significantly reduced [8]. To further prove this point, electrical impedance spectra (EIS) was measured at 0.9 V in dark, **Figure 2f**. In the Nyquist plot the GuaI-treated PSC larger circle, as compared with the one of the untreated PSC, represent a larger recombination resistance (R_{rec}), which is consistent with a reduction of charge recombination in the GuaI-treated PSC. Moreover, maximum power point tracking over 3000 s of both un encapsulated 1.58 eV and 1.72 eV and their shelf stability over 60 days was measured, **Figure S12**. Both devices show very stable output under 1 sun condition (AM 1.5) over 3000 s. The 1.58 eV PSCs kept ~90% efficiency and 1.72 eV PSCs kept ~93% efficiency after 60 days stocked in a dry box with around 35% humidity.

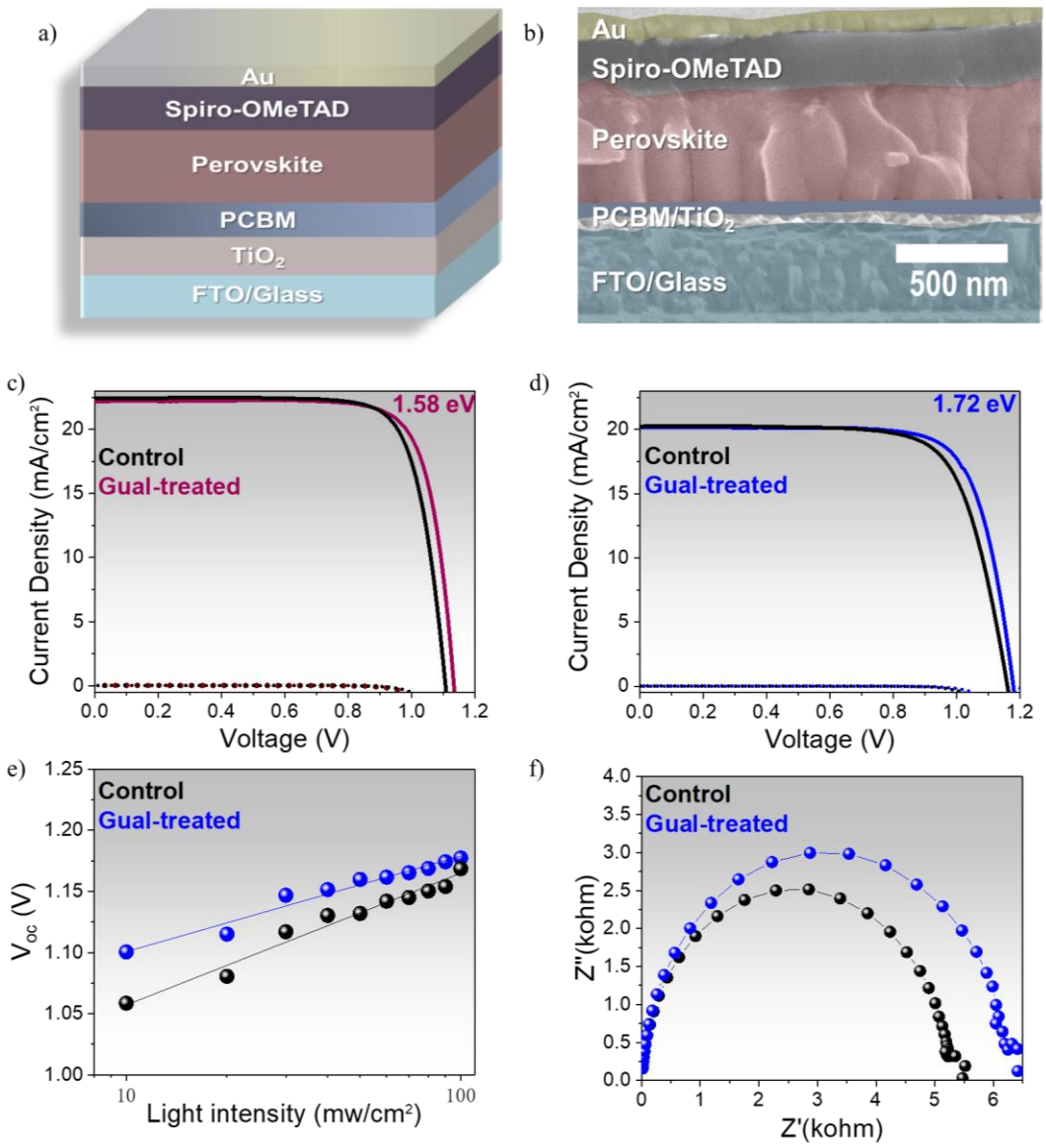

Figure 2. n-i-p planar 1.58 eV and 1.72 eV perovskite solar cells (PSCs) on glass with active area 0.16 $cm^{2.}$ a) PSCs layered architecture b) Cross sectional SEM image of 1.72 eV-based PSCs. c) J-V curves of untreated (control, black line) and GuaI-treated (brown line) 1.58 eV PSCs; d) J-V curves of untreated (control, black line) and GuaI-treated (blue line) 1.72 eV PSCs; e) 1.72 eV PSCs V_{oc} *vs* light intensity and f) Nyquist plot of untreated (control, black line) and GuaI-treated (blue line) 1.72 eV PSCs .

The low-temperature fabrication procedure guarantees high reproducibility and good efficiency also for flexible planar PSCs (PEN/ITO/TiO_2/PCBM/1.58 eV &1.72 eV perovskite /Spiro-OMeTAD/Au**).** J-V curves of untreated and GuaI-treated 1.58 eV PSCs showed the PCE improvement from 16.2% to 17.0%, **Figure 3a** and **Table 1**. The best performing 1.72 eV PSCs after the GuaI treatment also reached a PCE of 15.8% from 14.7%, **Figure 3b** and **Table 1.** The

narrow PCEs variation (± 0.6%) demonstrate the good devices' reproducibility, **Figure 3c**, the average PCE of GuaI-treated 1.58 eV PSCs and 1.72 eV PSCs were 16.1% and 15.1%, respectively. The photovoltaic parameters are shown in **Table 1**. Comparing the flexible PSCs with the rigid ones, the main loss in efficiency comes from a reduced J_{sc}. This is due to the lower optical transmittance of ITO/PEN in the UV-visible range as compared to FTO/glass, **Figure S13a**. The typical IPCE is shown in **Figure S13b**. The good quality of the TiO_2 ETL and of the perovskite films was proved by the good bending resistivity of both flexible 1.58 eV and 1.72 eV PSCs. Indeed, after 1000 bending cycles at bending radius of 10 mm, 1.58 eV and 1.72 eV PSCs show a marginal PCE drop of 12% and 6% PCE respectively, **Figure 3**d. The small PCE drop could be result from formation cracks in the ITO electrode as discussed earlier by Pandey et al.. [56, 57]

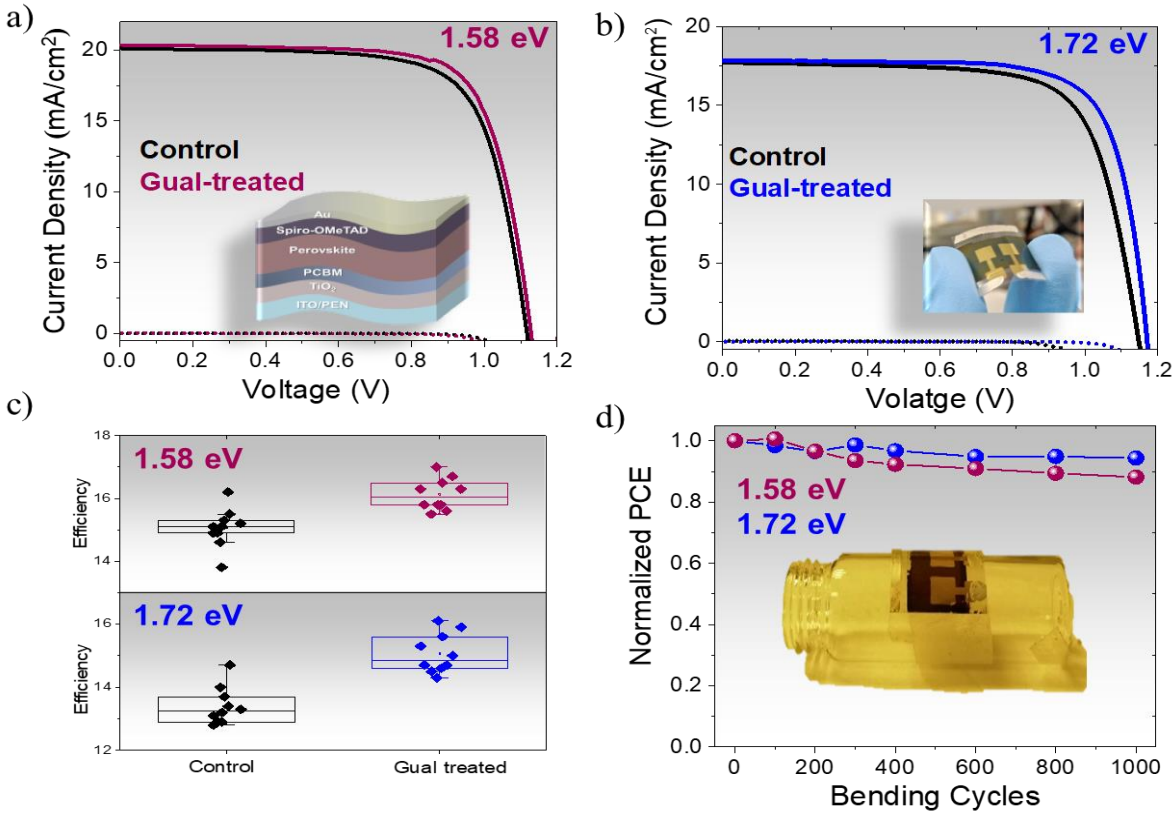

Figure 3. Flexible n-i-p planar 1.58 eV and 1.72 eV perovskite solar cells (PSCs) on PEN, active area 0.16 cm^2. Champion J-V curves of a) untreated (control, black line) and GuaI-treated (brown line) 1.58 eV PSCs and b) of untreated (control, black line) and GuaI-treated (blue line) 1.72 eV PSCs 1. c) PCE Statistical distribution of 10 flexible PSCs untreated (control, black line) and GuaI-treated (brown line) 1.58 eV PSCs (top panel) and untreated (control, black line) and GuaI-treated (blue line) 1.72 eV PSCs (bottom panel) d) Normalized PCE vs the bending cycles at radius of 10 mm for both GuaI-treated 1.58 eV PSCs and GuaI-treated 1.72 eV PSCs.

Table 1. Photovoltaic parameters of champion 1.58 eV and 1.72 eV PSCs before and after the GuaI treatment, 0.16 cm^2 area. The average efficiency over 10 PSCs is also reported as comparison.

Substrate	Bandgap (eV)	Treatment	J_{sc} (mA/cm^2)	V_{oc} (V)	FF (%)	η (%)	$η_{av}$ (%)
Glass	1.58	Control	22.4	1.10	78.2	**19.4**	19.1
		GuaI- treated	22.2	1.13	79.0	**19.8**	19.3
PEN	1.58	Control	20.1	1.12	72.3	**16.2**	15.1
		GuaI- treated	20.3	1.13	74.3	**17.0**	16.1
Glass	1.72	Control	20.3	1.16	73.0	**17.1**	15.7
		GuaI- treated	20.2	1.18	75.4	**18.0**	17.2
PEN	1.72	Control	17.7	1.15	72.2	**14.7**	13.4
		GuaI- treated	17.9	1.17	75.5	**15.8**	15.1

Scaling up the PSCs is essential for many industrial applications. We fabricated 1 cm^2 both 1.58 eV and 1.72 eV-PSCs on glass and PEN substrates. J-V curves of our champion 1 cm^2 1.58 eV-PSCs on glass achieved a PCE of 18.2% and 1.72 eV-PSCs on glass obtained a PCE of 16.6%, **Figure 4a**. The 1 cm^2 flexible 1.58 eV-PSCs reached high PCE of 16.2%, which is one the highest number reported. The very first flexible 1.72 eV-PSC also showed a very promising PCE of 13.9%, **Figure 4b**. The photovoltaic parameters are shown in **Table 2**. The main efficiency limitation in scaling the PSCs up is the *FF* reduction, ascribable to the high TCO resistances, while both V_{oc} and J_{sc} remain constant. These are promising conditions for further PCEs increase by just improving TCO conductivity and employing patterned substrates.

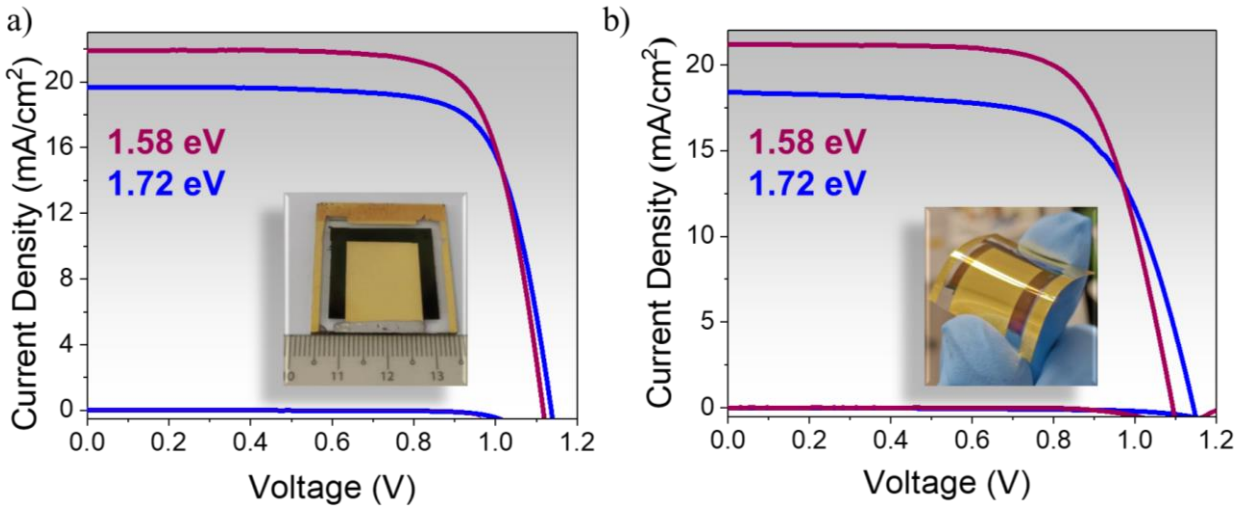

Figure 4. Large area, 1 cm^2, n-i-p planar perovskite solar cells (PSCs) on glass and on PEN. a) Champion J-V curves of rigid GuaI-treated 1.58 eV and GuaI-treated 1.72 eV PSCs. b) Champion J-V curves of flexible GuaI-treated 1.58 eV and GuaI-treated 1.72 eV PSCs under illumination (1 Sun, AM 1.5) and in dark.

Table 2. Photovoltaic parameters of large area, 1 cm^2, champion rigid and flexible GuaI- treated 1.58 eV and GuaI- treated 1.72 eV PSCs

Substrate	**Bandgap** (eV)	**J_{sc}** (mA/cm2)	**V_{oc}** (V)	***FF*** (%)	**η** (%)
Glass	1.58	21.9	1.12	74.6	**18.2**
PEN	1.58	21.2	1.09	70.1	**16.2**
Glass	1.72	19.7	1.14	74.7	**16.7**
PEN	1.72	18.4	1.14	66.2	**13.9**

Conclusion

In conclusion, we have introduced a new method for achieving high efficiency rigid and flexible PSCs based on low-temperature processed TiO_2 thin film as ETL and on guanidinium iodide passivation treatment of the perovskite layer to reduce the charge recombination losses. Indeed, we have demonstrated planar 1.58 eV and 1.72 eV PSCs achieving efficiencies as high as 19.8%

and 18.0 % on glass. At the same time, flexible PSCs showed efficiency of 17.0% and 15.8% for 1.58 eV and 1.72 eV-bandgap perovskites. Large area (1 cm^2) 1.58 eV- PSCs on both rigid and flexible substrate have reached high PCEs of 18.2% and 16.0%, 1.72 eV- PSCs on both rigid and, for the very first time on flexible substrate, have also achieved high PCEs of 16.7% and 13.9%, respectively. The high-performing low-temperature processed PSCs based on high-bandgap perovskite pave the way to the further development of tandem perovskite on Silicon and flexible perovskite on perovskite solar cells.

Experimental Section

TiO_2 thin film preparation

TiO_2 nanoparticles were prepared introducing modifications to procedures in refs [41, 42] to suspend have an ethanol suspension and using $TiCl_4$ as stabilizer. 1 ml $TiCl_4$ was slowly dropped in 4 ml anhydrous ethanol and 16 ml benzyl alcohol solution, then then kept in oven at 70 ^oC for 12 hours. The original reddish solution became slight yellow and then milky, proving the TiO_2 nanoparticles formation. 1 ml of TiO_2 suspension was diluted in 4 ml of dither ether and centrifuged at 5000 r.p.m. for 300s. TiO_2 nanoparticles collected at the bottom of the vial were re-dispersed in ethanol and dither ether and centrifuged 3 more times. TiO_2 nanoparticles were weighted and re-dispersed in pure anhydrous ethanol @ 10 mg/ml. As last stage, $TiCl_4$ solution was slowly dropped into TiO_2 suspension. TiO_2 suspension was spin-coated at 5000 on glass and heated at 150 ^oC for 1 hour and treated by UV-ozone for 20 minutes.

Material characterization

The XPS spectra was recorded by an X-ray photoelectron spectroscopy (XPS; Kratos AXIS Supra XPS). XRD patterns recorded using an X-ray diffraction (XRD; Bruker D8 Advance XRD**)**. The film morphology was characterized using SEM (FESEM; JEJOL JSM-7600F). TiO_2 thin film thicknesses were measured using an Alpha-step 500 surface profiler. UV-vis absorption and transmittance spectra were measurements n on a Hitachi U-3501 ultraviolet/visible/near-

infrared spectrophotometer. Steady photoluminescence spectra were measured by Spectro-fluorophotometer (Shimadzu, RF-5301PC), with 520 nm excitation. TRPL decays were collected using a micro-PL setup and a Picoquant PicoHarp 300 time-correlated single photon counting (TCSPC) system and a laser diode (Picoquant P-C-405B, λ = 405 nm, <2 $\mu J/cm^2$, 40 MHz) as excitation source. The fluorescence was collected by an avalanche diode synchronized with excitation laser via TCSPC electronic. The full width at half-maximum instrument response function is around 50 ps [58, 59].

Device fabrication and measurements

Nippon FTO glass (15Ω/sq) and ITO/PEN (15Ω/sq) was etched by Zn powder and HCl, and cleaned by 2% Hellmanex water solution, water and ethanol for 15 minutes and UV-ozone treated for 20 minutes. TiO_2 suspension was spun-coated on the cleaned substrates and PCBM, dissolved in chlorobenzene @ of 7.5 mg/ml, and spin coated on TiO_2 at 3000 r.p.m. for 30s. The samples were annealed at 100 ºC for 30 min. Double cation perovskite precursor was prepared by dissolving 1.105 M formamidinium iodide (FAI, Dyesol), 0.195 M CsI (Sigma-Aldrich, 99.999%), 0.88 M PbI_2 (TCI), and 0.52 M $PbBr_2$ (TCI) in anhydrous N, N-Dimethylformamide (DMF): Dimethyl sulfoxide (DMSO) 4:1 mixed solution and stirred overnight. Triple cation perovskite precursor was prepared by dissolving 1M FAI (Dyesol), 1.1 M PbI_2 (TCI), 0.2 M MABr (Dyesol) and 0.2 M $PbBr_2$ (TCI) in anhydrous DMF (Sigma-Aldrich): DMSO (Sigma-Aldrich) 4:1. Then 0.065 M CsI, pre-dissolved as a 1.5 M stock solution in DMSO. The precursor solution was spin-coated at 1000 r.p.m for 10 s and then 6000 r.p.m for 20 s and 100 μL of chlorobenzene was casted onto the substrate 5 s before end. The films annealed @100 °C for 1 hour. Different amounts of Guanidinium iodide were dissolved in 2-propanol (5, 10, 15, 20, 40 mM) and spin-coated onto perovskite film at 3000 r.p.m., then annealed @ 100ºC for 10 min.

The optimized concentration has been proved to be 5 mM. HTL solution was prepared by dissolving 72.3 mg Spiro-OMeTAD (Sigma-Aldrich), 28.5 μL 4-tert-butylpyridine (Sigma-Aldrich,96%), and 17.5 μL bis(trifluoromethane)sulfonimide lithium salt (Sigma-Aldrich) solution (520 mg Li-TFSI in 1 mL acetonitrile) in 1 mL chlorobenzene and then spin-casted the on the perovskite layer at 4000 rpm for 30 s. A 100 nm Au electrode was thermally evaporated on top of HTL (evaporating rate 0.1 Å/s for the first 10 nm and then 1 Å/s for the following 90 nm).

The current density–voltage (J–V) curves were measured under AM 1.5 sunlight (94011A-ES, ABB). The effective mask area is 0.16 cm^2 and 1 cm^2. The incident photon-to-current conversion efficiency (IPCE) was measured by using a PVE300 (Bentham), with xenon/quartz halogen light source in DC mode. The EIS spectra and maximum power point (MPP) track are measured by an Autolab machine (PGSTAT302N, Software version- NOVA 1.11).

Supporting Information

Supporting Information is available from the ACS publication website at DOI: XXX.

Acknowledgements

This research is supported by the National Research Foundation, Prime Minister's Office, Singapore under Energy Innovation Research Program (Grant number, NRF2015EWT-EIRP003-004 and NRF-CRP14-2014-03 and Solar CRP: S18-1176-SCRP)

Received: ((will be filled in by the editorial staff))
Revised: ((will be filled in by the editorial staff))
Published online: ((will be filled in by the editorial staff))

References

[1] Im, J. H.; Lee, C. R.; Lee, J. W.; Park, S. W.; Park, N. G. 6.5% Efficient Perovskite Quantum-dot-sensitized Solar Cell, *Nanoscale*, **2011**, 3, 4088-4093.

[2] Dong, Q. F.; Fang, Y. J.; Shao, Y. C.; Mulligan, P.; Qiu, J.; Cao, L.; Huang, J. S. Electron-hole Diffusion Lengths> 175 μm in Solution-grown $CH_3NH_3PbI_3$ Single Crystals, **2015**, 347, 967-970.

[3] Noh, J. H.; Im, S. H.; Heo, J. H.; Mandal, T. N.; Seok, S. I. Chemical Management for Colorful, Efficient, and Stable Inorganic–organic Hybrid Nanostructured Solar Cells, *Nano lett.*, **2013**, 13, 1764-1769.

[4] Ball, J. M.; Lee, M. M.; Hey, A.; Snaith, H. J. Low-temperature Processed Meso-superstructured to Thin-film Perovskite Solar Cells, *Energy Environ. Sci.*, **2013**, 6, 1739.

[5] Kojima, A.; Teshima, K.; Shirai, Y.; Miyasaka, T. Organometal Halide Perovskites as Visible-Light Sensitizers for Photovoltaic Cells, *J. Am. Chem. Soc.*, **2009**, 131, 6050.

[6] Jeon, N. J.; Na, H.; Jung, E. H.; Yang, T. Y.; Lee, Y. G.; Kim, G.; Shin, H. W.; Seok, S. I.; Lee, J.; Seo, J. A Fluorene-terminated Hole-transporting Material for Highly Efficient and Stable Perovskite Solar Cells, *Nat. Energy*, **2018**, 3, 682-689.

[7] Jung, E. H.; Jeon, N. J.; Park, E. Y.; Moon, C. S.; Shin, T. J.; Yang, T.-Y.; Noh, J. H.; Seo, J. Efficient, stable and scalable perovskite solar cells using poly (3-hexylthiophene). *Nature*, **2019**, 567, 511.

[8] Jiang, Q.; Zhao, Y.; Zhang, X.; Yang, X.; Chen, Y.; Chu, Z.; Ye, Q.; Li, X.; Yin, Z.; You, J. Surface passivation of perovskite film for efficient solar cells. *Nature Photonics*, **2019**, 13, 460-466.

[9] Feng, J.; Zhu, X.; Yang, Z.; Zhang, X.; Niu, J.; Wang, Z.; Zuo, S.; Priya, S.; Liu, S. F.; Yang, D. Record Efficiency Stable Flexible Perovskite Solar Cell Using Effective Additive Assistant Strategy, *Adv. Mater.*, **2018**, 30, e1801418.

[10] Wang, C.; Guan, L.; Zhao, D.; Yu, Y.; Grice, C. R.; Song, Z.; Awni, R. A.; Chen, J.; Wang, J.; Zhao, X.; Yan, Y. *ACS Energy Lett.,* **2017**, 2, 2118-2124.

[11] Kumar, M. H.; Yantara, N.; Dharani, S.; Graetzel, M.; Mhaisalkar, S.; Boix, P. P. Mathews, N., Flexible, Low-temperature, Solution processed ZnO-based Perovskite Solid State Solar Cells, *Chem. Commun.*, **2013**, 49, 11089-11091.

[12] Docampo, P.; Ball, J. M.; Darwich, M.; Eperon, G. E.; Snaith, H. J.; Efficient Organometal Trihalide Perovskite Planar-heterojunction Solar Cells on Flexible Polymer Substrates, *Nat. comm.*, **2013**, 4, 2761.

[13] Yang, D.; Yang, R.; Zhang, J.; Yang, Z.; Liu, S.; Li, C.; High Efficiency Flexible Perovskite Solar Cells Using Superior Low Temperature TiO_2, *Energy Environ. Sci.*, **2015**, 8, 3208-3214.

[14] Giacomo, F. D., Zardetto, V.; D'Epifanio, A.; Pescetelli, S.; Matteocci, F.; Razza, S.; Di Carlo, A.; Licoccia, S.; Kessels, W. M.; Creatore, M.; Flexible Perovskite Photovoltaic Modules and Solar Cells Based on Atomic Layer Deposited Compact Layers and UV-Irradiated TiO_2 Scaffolds on Plastic Substrates, *Adv. Energy Mater.*, **2015**, 5, 1401808.

[15] You, J. B.; Hong, Z. R.; Yang, Y.; Chen, Q.; Cai, M.; Song, T. B.; Chen, C. C.; Lu, S. R.; Liu, Y. S.; Zhou, H. P.; Yang, Y.; Low-temperature Solution-processed Perovskite Solar Cells with High Efficiency and Flexibility, *ACS nano,* **2014**, 8, 1674-1680.

[16] Roldán-Carmona, C.; Malinkiewicz, O.; Soriano, A.; Mínguez Espallargas, G.; Garcia, A.; Reinecke, P.; Kroyer, T.; Dar, M. I.; Nazeeruddin, M. K.; Bolink, H. J.; Flexible High Efficiency Perovskite Solar Cells, *Energ. Environ. Sci.*, **2014**, 7, 994.

[17] Yin, X.; Chen, P.; Que, M.; Xing, Y.; Que, W.; Niu, C.; Shao, J.; Highly Efficient Flexible Perovskite Solar Cells Using Solution-Derived NiO_x Hole Contacts, *ACS nano*, **2016**, 10, 3630-3636.

[18] Zhang, H.; Cheng, J.; Lin, F.; He, H.; Mao, J.; Wong, K. S.; Jen, A. K.Y.; Choy, W. C.; Pinhole-Free and Surface-Nanostructured NiO_x Film by Room-Temperature Solution Process for High-Performance Flexible Perovskite Solar Cells with Good Stability and Reproducibility, *ACS nano*, **2015**, 10, 1503-1511.

[19] Najafi, M.; Giacomo, F. D.; Zhang, D.; Shanmugam, S.; Senes, A.; Verhees, W.; Hadipour, A.; Galagan, Y.; Aernouts, T.; Veenstra, S.; Andriessen, R., Highly Efficient and Stable Flexible Perovskite Solar Cells with Metal Oxides Nanoparticle Charge Extraction Layers, *Small*, **2018**, 14, 1702775.

[20] Hou, L.; Wang, Y.; Liu, X.; Wang, J.; Wang, L.; Li, X.; Fu, G.; Yang, S. 18.0% efficiency flexible perovskite solar cells based on double hole transport layers and $CH_3NH_3PbI_{3-x}Cl_x$ with dual additives. *J. Mater. Chem. C*, **2018**, 6, 8770-8777.

[21] Liu, D.; Kelly, T. L. Perovskite Solar Cells with a Planar Heterojunction Structure Prepared Using Room-temperature Solution Processing Techniques, *Nat. Photonics*, **2013**, 8, 133-138.

[22] Shin, S. S.; Yang, W. S.; Noh, J. H.; Suk, J. H.; Jeon, N. J.; Park, J. H.; Kim, J. S.; Seong, W. M.; Seok, S. I. High-performance Flexible Perovskite Solar Cells Exploiting Zn_2SnO_4 Prepared in Solution Below 100 °C, *Nat. commun.*, **2015**, 6, 7410.

[23] Mali, S. S.; Hong, C. K.; Inamdar, A.; Im, H.; Shim, S. E.; Efficient Planar nip Type Heterojunction Flexible Perovskite Solar Cells with Sputtered TiO_2 Electron Transporting Layers, *Nanoscale*, **2017**, 9, 3095-3104.

[24] Park, M.; Kim, J. Y.; Son, H. J.; Lee, C. H.; Jang, S. S.; Ko, M. J. Low-temperature Solution-processed Li-doped SnO_2 as an Effective Electron Transporting Layer for High-performance Flexible and Wearable Perovskite Solar cells, *Nano Energy*, **2016**, 26, 208-215.

[25] Park, S. Y.; Baek, M. Y.; Ju, Y. K.; Kim, D. H.; Moon, C. S.; Noh, J. H.; Jung, H. S. Simultaneous Ligand Exchange Fabrication of Flexible Perovskite Solar Cells using Newly Synthesized Uniform Tin Oxide Quantum Dots, *J. Phys. Chem. Lett.*, **2018,** 9, 5460-5467.

[26] Yang, D.; Yang, R.; Wang, K.; Wu, C.; Zhu, X.; Feng, J.; Ren, X.; Fang, G.; Priya, S.; Liu, S. F. High Efficiency Planar-type Perovskite Solar Cells with Negligible Hysteresis Using EDTA-Complexed SnO_2, *Nat. Commun.*, **2018**, 9, 3239.

[27] Liu, C.; Zhang, L.; Zhou, X.; Gao, J.; Chen, W.; Wang, X.; Xu, B., Hydrothermally Treated SnO2 as the Electron Transport Layer in High‐Efficiency Flexible Perovskite Solar Cells with a Certificated Efficiency of 17.3%. *Adv. Funct. Mater.*, **2019**, 1807604.

[28] Zhong, M.; Liang, Y.; Zhang, J.; Wei, Z.; Li, Q.; Xu, D., Highly efficient flexible $MAPbI_3$ solar cells with a fullerene derivative-modified SnO_2 layer as the electron transport layer. *J Mater. Chem. A,* **2019,** 7, 6659.

[29] Bu, T.; Li, J.; Zheng, F.; Chen, W.; Wen, X.; Ku, Z.; Peng, Y.; Zhong, J.; Cheng, Y.-B.; Huang, F., Universal passivation strategy to slot-die printed SnO_2 for hysteresis-free efficient flexible perovskite solar module. *Nature comm.,* **2018,** *9,* 4609.

[30] Mali, S. S.; Hong, C. K.; Inamdar, A. I.; Im, H.; Shim, S. E. Efficient Planar Nip Type Heterojunction Flexible Perovskite Solar Cells with Sputtered TiO_2 Electron Transporting Layers, *Nanoscale*, **2017**, 9, 3095-3104.

[31] Giacomo, F. D.; Zardetto, V.; D'Epifanio, A.; Pescetelli, S.; Matteocci, F.; Razza, S.; Di Carlo, A.; Licoccia, S.; Kessels, W. M. M.; Creatore, M.; Brown, T. M. Flexible Perovskite

Photovoltaic Modules and Solar Cells Based on Atomic Layer Deposited Compact Layers and UV-Irradiated TiO_2 Scaffolds on Plastic Substrates, *Adv. Energy Mater.*, **2015**, 5, 1401808.

[32] Zardetto, V.; Giacomo, F. D.; Lucarelli, G.; Kessels, W. M. M.; Brown, T. M. Creatore M., Plasma-assisted Atomic Layer Deposition of TiO_2 Compact Layers for Flexible Mesostructured Perovskite Solar Cells, *Sol. Energy*, **2017**, 150, 447-453.

[33] Qiu, W.; Paetzold, U. W.; Gehlhaar, R.; Smirnov, V.; Boyen, H. G.; Tait, J. G.; Conings B., Zhang W., Nielsen C. B., McCulloch I., Froyen L., Heremans P., Cheyns D., An Electron Beam Evaporated TiO_2 Layer for High Efficiency Planar Perovskite Solar Cells on Flexible Polyethylene Terephthalate Substrates, *J. Mater. Chem. A*, **2015**, 3, 22824-22829.

[34] Feleki, B.; Bex, G.; Andriessen, R.; Galagan, Y.; Giacomo, F. D. Rapid and Low Temperature Processing of Mesoporous TiO_2 for Perovskite Solar Cells on Flexible and Rigid Substrates, *Mater. Today Comm.*, **2017**, 13, 232-240.

[35] Jeong, I.; Jung, H.; Park, M.; Park, J. S.; Son, H. J.; Joo, J.; Lee, J.; Ko, M. J. A Tailored TiO_2 Electron Selective Layer for High-performance Flexible Perovskite Solar Cells via Low Temperature UV Process, *Nano Energy*, **2016**, 28, 380-389.

[36] Zhou, Y. Q.; Wu, B. S.; Lin, G. H.; Xing, Z.; Li, S. H.; Deng, L. L.; Chen, D. C.; Yun, D. Q.; Xie, S. Y. Interfacing Pristine C60 onto TiO_2 for Viable Flexibility in Perovskite Solar Cells by a Low-Temperature All-Solution Process, *Adv. Energy Mater.*, **2018**, 8, 1800399.

[37] Hossain, I. M.; Hudry, D.; Mathies, F.; Abzieher, T.; Moghadamzadeh, S.; Rueda-Delgado, D.; Schackmar, F.; Bruns, M.; Andriessen, R.; Aernouts, T. Scalable Processing of Low-Temperature TiO_2 Nanoparticles for High-Efficiency Perovskite Solar Cells. *ACS Applied Energy Materials* **2018,** *2* (1), 47-58.

[38] McMeekin, D. P.; Sadoughi, G.; Rehman, W.; Eperon, G. E.; Saliba, M.; Hörantner, M. T.; Haghighirad, A.; Sakai, N.; Korte, L.; Rech, B. A Mixed-cation Lead Mixed-halide Perovskite Absorber for Tandem Solar Cells, *Science*, **2016**, 351, 151-155.

[39] Zhou, Y.; Wang, F.; Cao, Y.; Wang, J. P.; Fang, H. H.; Loi, M. A.; Zhao, N.; Wong, C. P. Benzylamine-treated Wide-bandgap Perovskite with High Thermal-photostability and Photovoltaic Performance, *Adv. Energy Mater.*, **2017**, 7, 1701048.

[40] Jiang, H.; Feng, J.; Zhao, H.; Li, G.; Yin, G.; Han, Y.; Yan, F.; Liu, Z.; Liu, S. Z. Low Temperature Fabrication for High Performance Flexible $CsPbI_2Br$ Perovskite Solar Cells, *Adv. Sci.*, **2018**, 1801117.

[41] Palmstrom, A. F.; Eperon, G. E.; Leijtens, T.; Prasanna, R.; Habisreutinger, S. N.; Nemeth, W.; Gaulding, E. A.; Dunfield, S. P.; Reese, M.; Nanayakkara, S., Enabling Flexible All-Perovskite Tandem Solar Cells. *Joule* **2019,** 9, 2193-2204.

[42] Tan, H. R.; Jain, A.; Voznyy, O.; Lan, X. Z.; de Arquer, F. P. G.; Fan, J. Z.; Quintero-Bermudez, R.; Yuan, M. J.; Zhang, B.; Zhao, Y. C.; Fan, F. J.; Li, P. C.; Quan, L. N.; Zhao, Y. B.; Lu, Z. H.; Yang, Z. Y.; Hoogland, S.; Sargent, E. H. Efficient and Stable Solution-processed Planar Perovskite Solar Cells via Contact Passivation, *Science*, **2017**, 355, 722-726.

[43] Wojciechowski, K.; Saliba, M.; Leijtens, T.; Abate, A.; Snaith, H. J.; Sub-150 ^{o}C Processed Meso-superstructured Perovskite Solar Cells with Enhanced Efficiency, *Energy Environ. Sci.*, **2014**, 7, 1142-1147.

[44] Pham, N. D.; Tiong, V. T.; Yao, D.; Martens, W.; Guerrero, A.; Bisquert, J.; Wang, H., Guanidinium thiocyanate selective Ostwald ripening induced large grain for high performance perovskite solar cells. *Nano Energy* **2017,** *41*, 476-487.

[45] Odlowski, A. D.; Roldán-Carmona, C.; Grancini, G.; Salado, M.; Ralaiarisoa, M.; Ahmad, S.; Koch, N.; Camacho, L.; De Miguel, G.; Nazeeruddin, M. K., Large guanidinium cation mixed with methylammonium in lead iodide perovskites for 19% efficient solar cells. *Nat. Energy* **2017,** *2* (12), 972.

[46] De Marco, N.; Zhou, H.; Chen, Q.; Sun, P.; Liu, Z.; Meng, L.; Yao, E.-P.; Liu, Y.; Schiffer, A.; Yang, Y., Guanidinium: a route to enhanced carrier lifetime and open-circuit voltage in hybrid perovskite solar cells. *Nano lett.* **2016,** *16* (2), 1009-1016.

[47] Alharbi, E. A.; Dar, M. I.; Arora, N.; Alotaibi, M. H.; Alzhrani, Y. A.; Yadav, P.; Tress, W.; Alyamani, A.; Albadri, A.; Zakeeruddin, S. M., Perovskite Solar Cells Yielding Reproducible Photovoltage of 1.20 V. *Research* **2019,** *2019*, 8474698.

[48] Pham, N. D.; Zhang, C.; Tiong, V. T.; Zhang, S.; Will, G.; Bou, A.; Bisquert, J.; Shaw, P. E.; Du, A.; Wilson, G. J.; Wang, H., Tailoring Crystal Structure of $FA_{0.83}Cs_{0.17}PbI_3$ Perovskite Through Guanidinium Doping for Enhanced Performance and Tunable Hysteresis of Planar Perovskite Solar Cells. *Adv. Funct. Mater.* **2019,** *29* (1), 1806479.

[49] Stoddard, R. J.; Rajagopal, A.; Palmer, R. L.; Braly, I. L.; Jen, A. K. Y.; Hillhouse, H. W., Enhancing Defect Tolerance and Phase Stability of High-Bandgap Perovskites via Guanidinium Alloying. *ACS Energy Lett.* **2018,** *3* (6), 1261-1268.

[50] Niederberger, M. Nonaqueous sol–gel routes to metal oxide nanoparticles. *Accounts of chemical research* **2007,** *40* (9), 793-800.

[51] Wilson, G. J.; Matijasevich, A. S.; Mitchell, D. R. G.; Schulz, J. C.; Will, G. D. Modification of TiO_2 for Enhanced Surface Properties: Finite Ostwald Ripening by a Microwave Hydrothermal Process, *Langmuir* **2006**, 22, 2016-2027.

[52] Cho, A.N.; Jang, I. H.; Seo, J. Y.; Park, N. G. Dependence of Hysteresis on the Perovskite Film Thickness: Inverse Behavior between TiO_2 and PCBM in a Normal Planar Structure, *J. Mater. Chem. A*, **2018,** *6*, 18206-18215.

[53] Chiang, C. H.; Tseng, Z. L.; Wu, C. G. Planar Heterojunction Perovskite/$PC_{71}BM$ Solar Cells with Enhanced Open-circuit Voltage via a (2/1)-step Spin-coating Process, *J. Mater. Chem. A*, **2014**, 2, 15897-15903.

[54] Kegelmann, L.; Wolff, C. M.; Awino, C.; Lang, F.; Unger, E. L.; Korte, L.; Dittrich, T.; Neher, D.; Rech, B.; Albrecht, S. Solution Processed Nano-ZnMgO Interfacial Layer for Highly Efficient Inverted Perovskite Solar Cells, *ACS appl. Mater. Inter.*, **2017**, 9, 17246-17256.

[55] Bruno, A.; Reynolds, L.X.; Dyer-Smith, C.; Nelson, J.; Haque, S.A.; Determining the exciton diffusion length in a polyfluorene from ultrafast fluorescence measurements of polymer/fullerene blend films. *J. Phy. Chem. C* **2013**, 117, 19832.

[56] Pandey, M.; Wang, Z.; Kapil, G.; Baranwal, A. K.; Hirotani, D.; Hamada, K.; Hayase, S., Dependence of ITO-Coated Flexible Substrates in the Performance and Bending Durability of Perovskite Solar Cells. Advanced Engineering Materials **2019**, 21, 1900288.

[57] Pandey, M.; Kapil, G.; Sakamoto, K.; Hirotani, D.; Kamrudin, M. A.; Wang, Z.; Hamada, K.; Nomura, D.; Kang, H.-G.; Nagayoshi, H., Efficient, hysteresis free, inverted planar flexible perovskite solar cells via perovskite engineering and stability in cylindrical encapsulation. Sustainable Energy & Fuels **2019**, 3, 1739-1748.

[58] Cortecchia, D.; Lew, K. C.; So, J. K.; Bruno, A.; Soci, C. Cathodoluminescence of Self-Organized Heterogeneous Phases in Multidimensional Perovskite Thin Films, *Chem. Mater.*, **2017**, 29 (23), 10088

[59] Bruno, A.; Cortecchia, D.; Chin, X. Y.; Fu, K.; Boix, P.; Soci, C. Temperature and Electrical Poling Effects on Ionic Motion in $MAPbI_3$ Photovoltaic Cells, *Adv. Energy Mater.*, **2017**, 7, 1700265.

Supporting Information

Interlayers Engineering for Flexible Large-Area Planar Perovskite Solar Cells

Jia Li, [1] *Guifang Han,* [1] *Kurt Vergeer,* [1] *Herlina Arianita Dewi,* [1] *Hao Wang,* [1] *Subodh Mhaisalkar,* [1, 2] *Annalisa Bruno,*[1]* *Nripan Mathews* [1, 2]

[1] *Energy Research Institute @ Nanyang Technological University (ERI@N)*

Research Techno Plaza, X-Frontier Block, Level 5, 50 Nanyang Drive 637553, Singapore

[2] *School of Materials Science and Engineering, Nanyang Technological University*

50 Nanyang Avenue 639798, Singapore

Corresponding Author

* Email: Annalisa@ntu.edu.sg

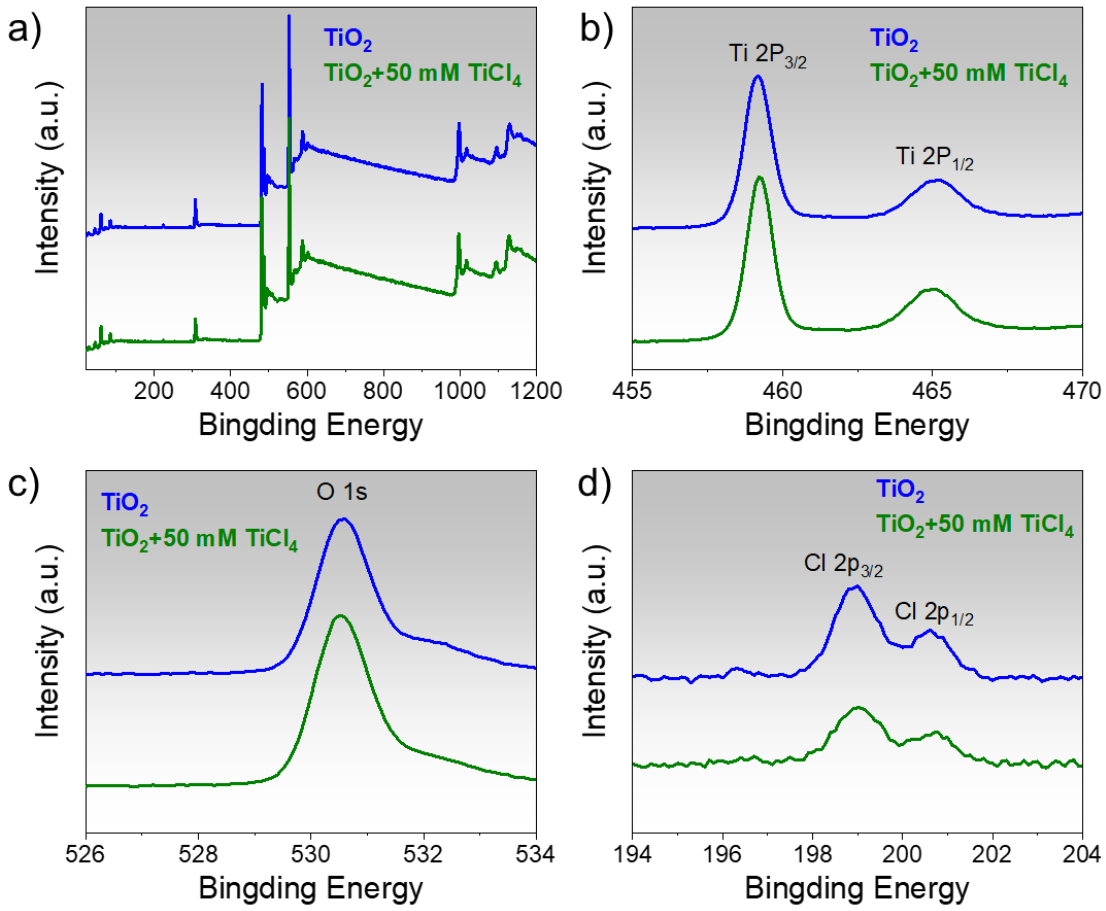

Figure S1. XPS spectra of TiO_2 and $TiCl_4$-terated TiO_2 films a) full spectra, b) Ti 2p, (c) O 1s, and (d) Cl 2p.

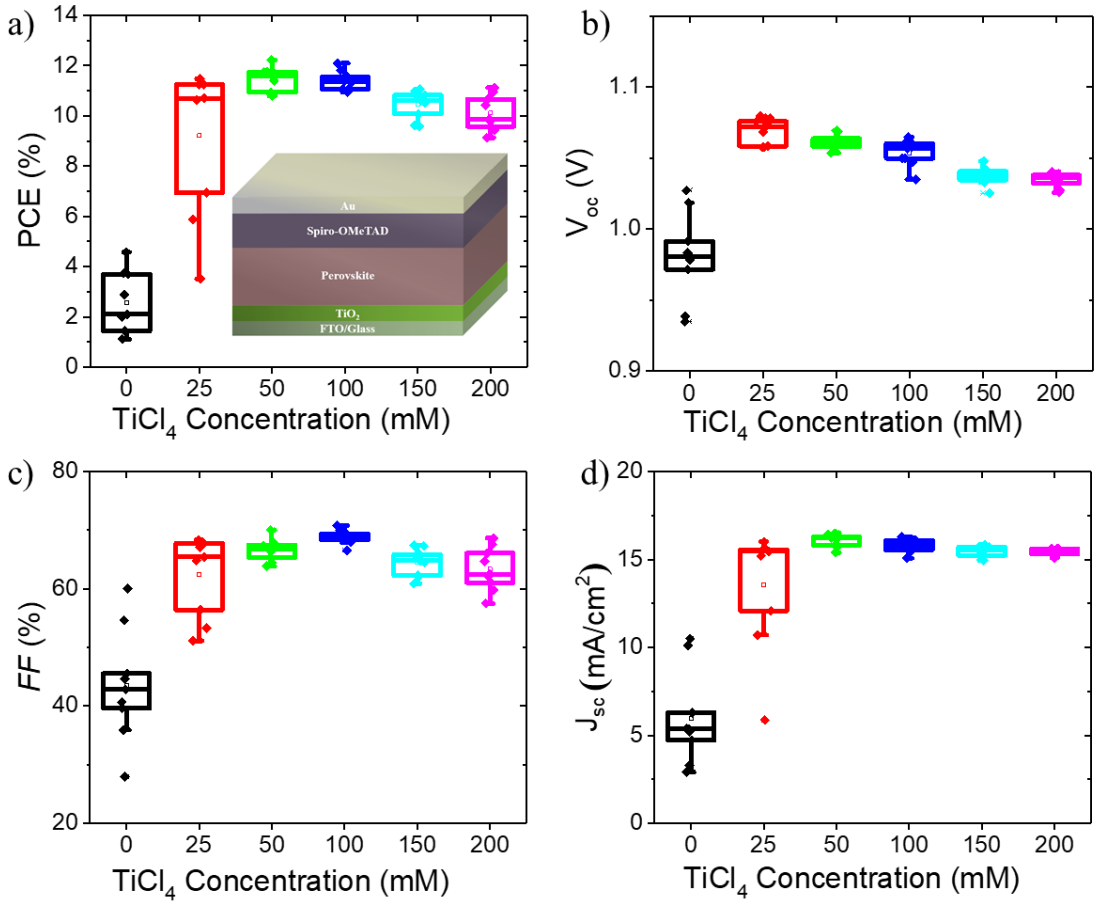

Figure S2. N-i-p planar 1.72 eV perovskite solar cells (PSCs) on glass with active area 0.16 cm^2, the compact TiO_2 layer quality was optimized to by varying $TiCl_4$ addition and so the $TiCl_4$ concentrations varied from 0 to 200 mM in the TiO_2 dispersion. The highest PCEs (~12%) were obtained for $TiCl_4$ concentrations 50 mM, while for higher ones the excess of Cl^- ligands leads to a reduction of film conductivity,Statistics data over 9 PSCs for each $TiCl_4$ concentration: a) PCEs, the PSCs layered structure is reported in the inset), b) V_{oc}, c) *FF* and d) J_{sc} distribution.

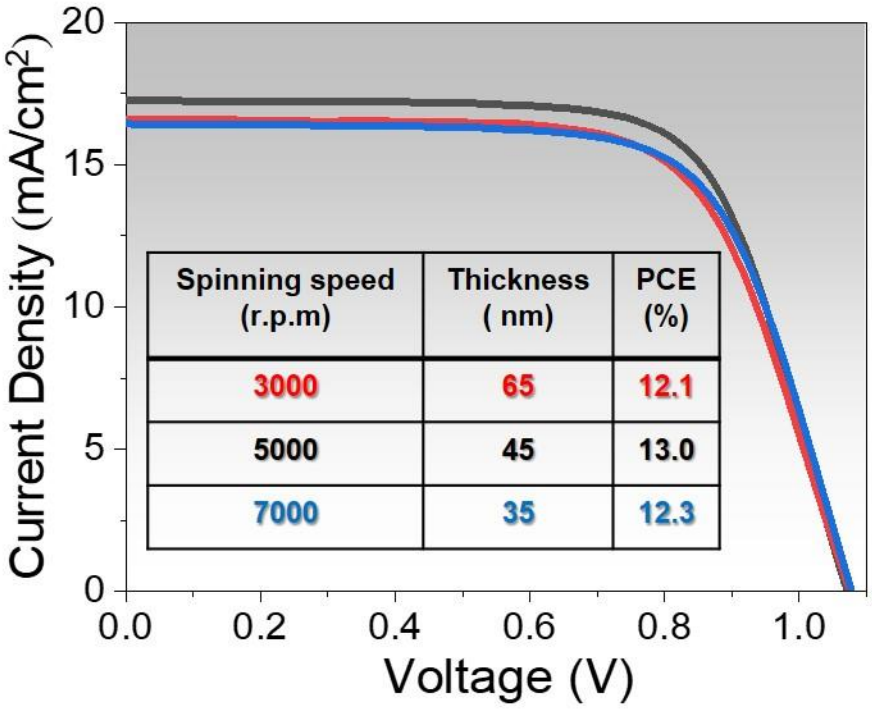

Figure S3. N-i-p planar 1.72 eV perovskite solar cells (PSCs) on glass with active area 0.16 cm^2, the compact TiO_2 layer thickness was tuned by varing spinning speed of TiO_2 suspension with 50 mM $TiCl_4$. J-V curves of PSCs based varing TiO_2 thickness, inset table show TiO_2 thickness and their coresponding PCE.

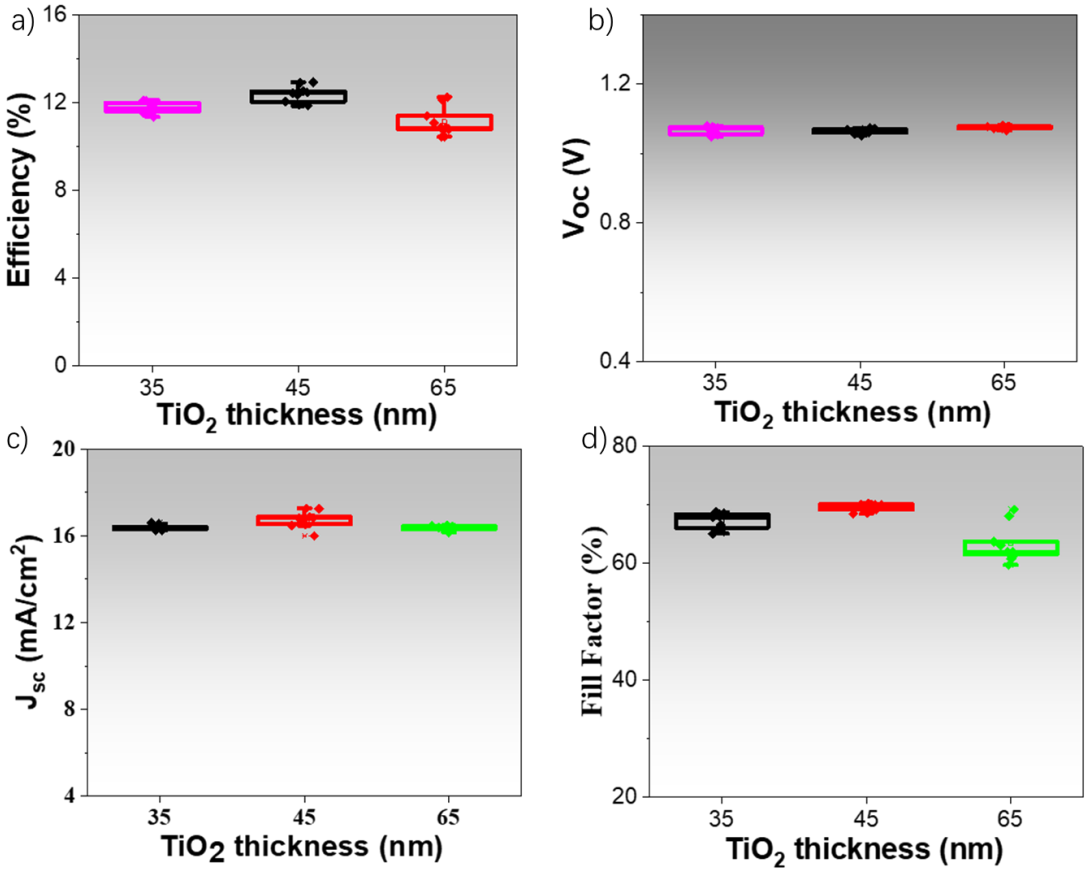

Figure S4. N-i-p planar ~1.72 eV perovskite solar cells (PSCs) on glass with active area 0.16 cm^2, the compact TiO_2 thickness was optimized to by varying spin-coating speed. The highest PCEs (~13%) were obtained for TiO_2 thickness of ~45 nm,Statistics data over 9 PSCs for each TiO_2 thickness: a) PCEs, the PSCs layered structure is reported in the inset), b) V_{oc}, c) J_{sc} and d) *FF* distribution.

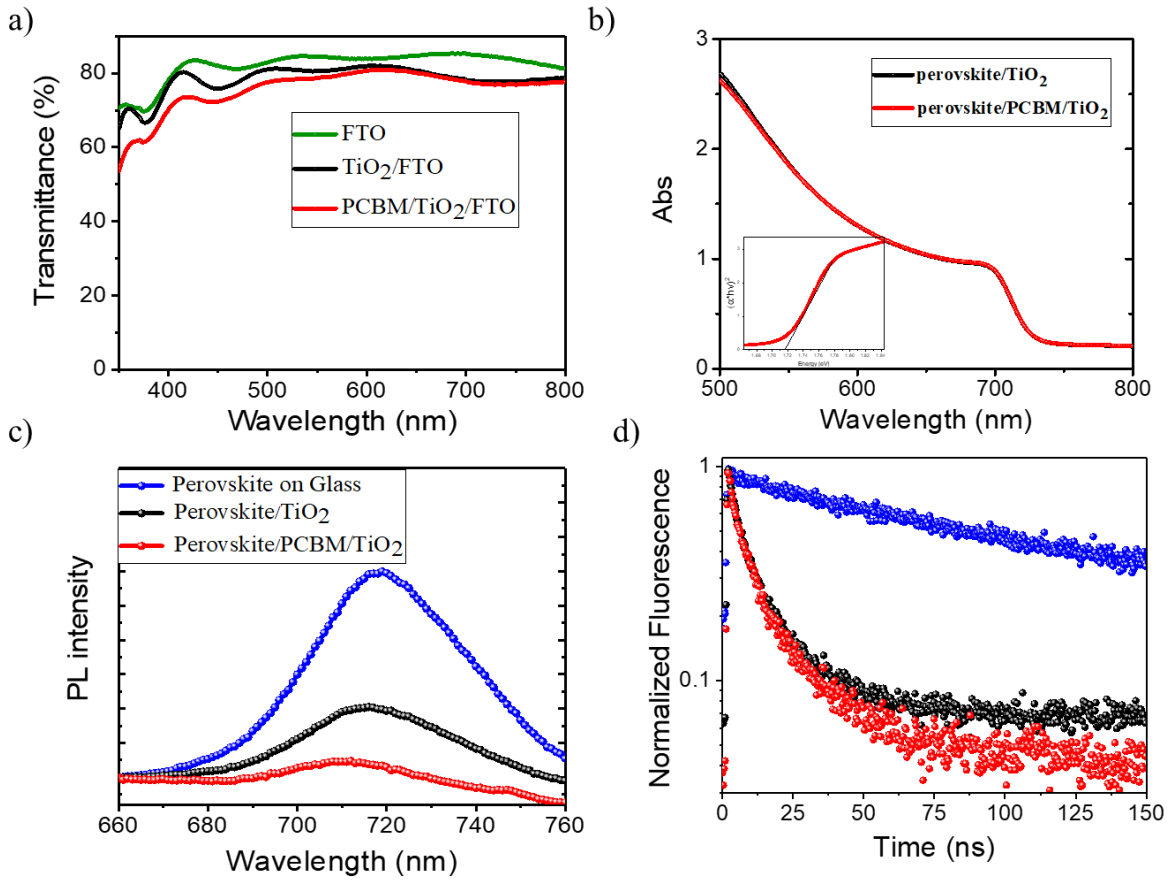

Figure S5. Characterization of $Cs_{0.15}FA_{0.85}Pb(I_{0.7}Br_{0.3})_3$ thin film on FTO, TiO_2 and PCBM/TiO_2. a) transmittance spectra of FTO, TiO_2/FTO and PCBM/TiO_2/FTO substrates, b) absorption spectra of perovskite layer deposited on TiO_2/FTO and PCBM/TiO_2/FTO, c) steady state and d) time-resolved PL spectra of perovskite on glass, TiO_2/FTO and PCBM/TiO_2/FTO substrates.

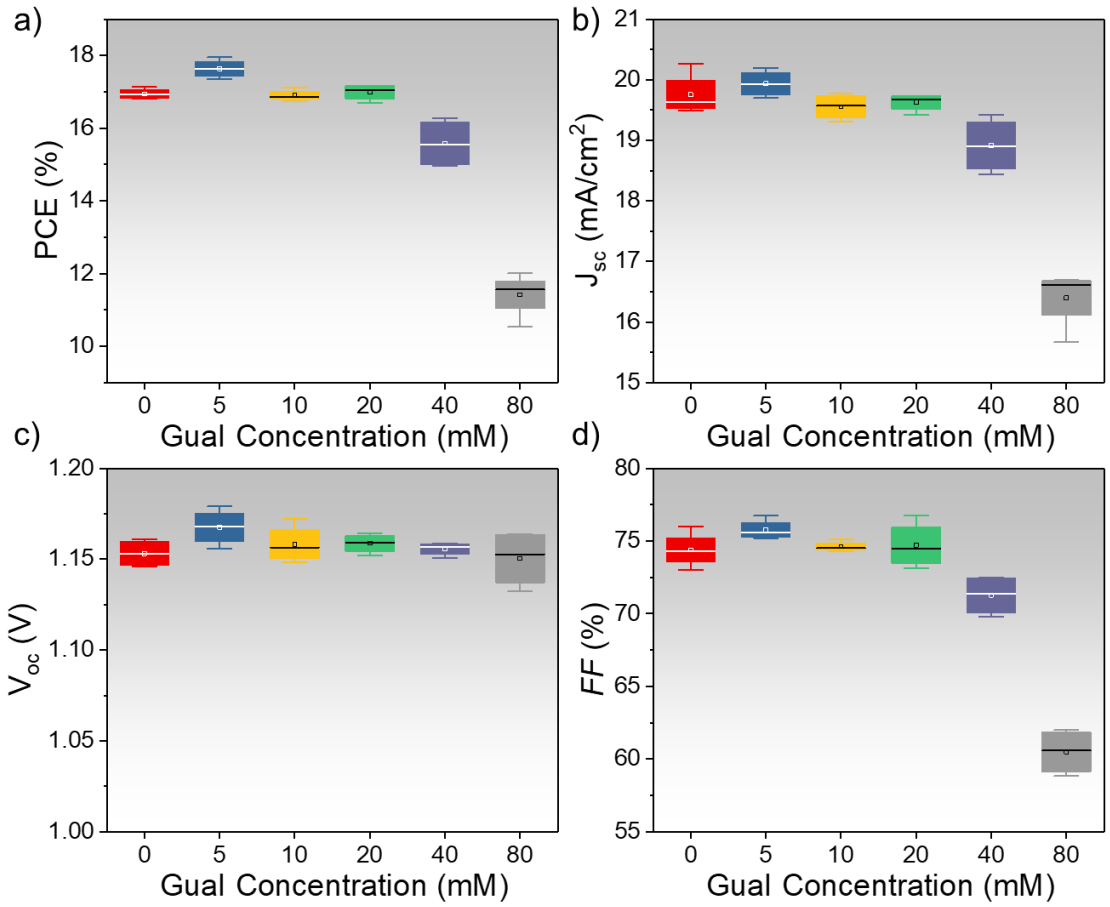

Figure S6. Photovoltaics performances of n-i-p planar 1.72 eV perovskite solar cells (PSCs) as function of guanidium iodide (GuaI) passivation concentration (from 0 to 80 mM): a) efficiency, b) J_{sc}, c) V_{oc} and d) Fill Factor. The highest effciencies (~18%) were obtained for GuaI concentrations 5 mM.

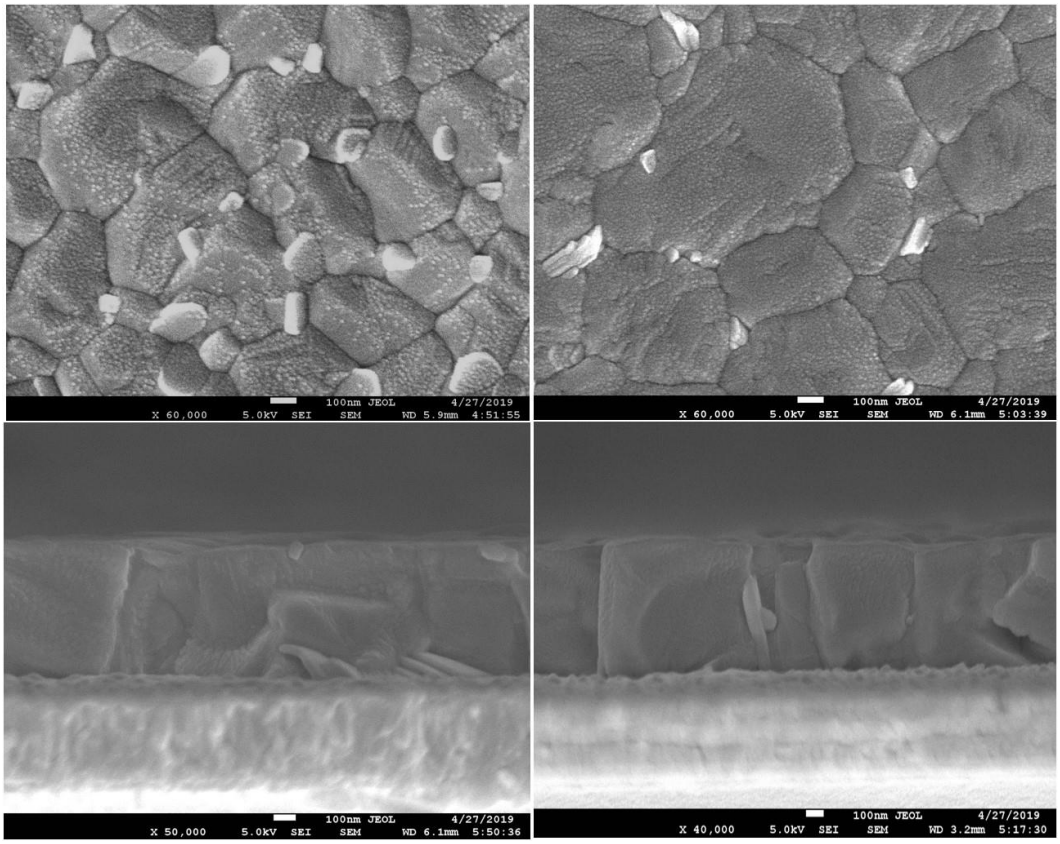

Figure S7. Top view and cross-sectional SEM images of 1.72 eV perovskite film before and after GuaI treatment.

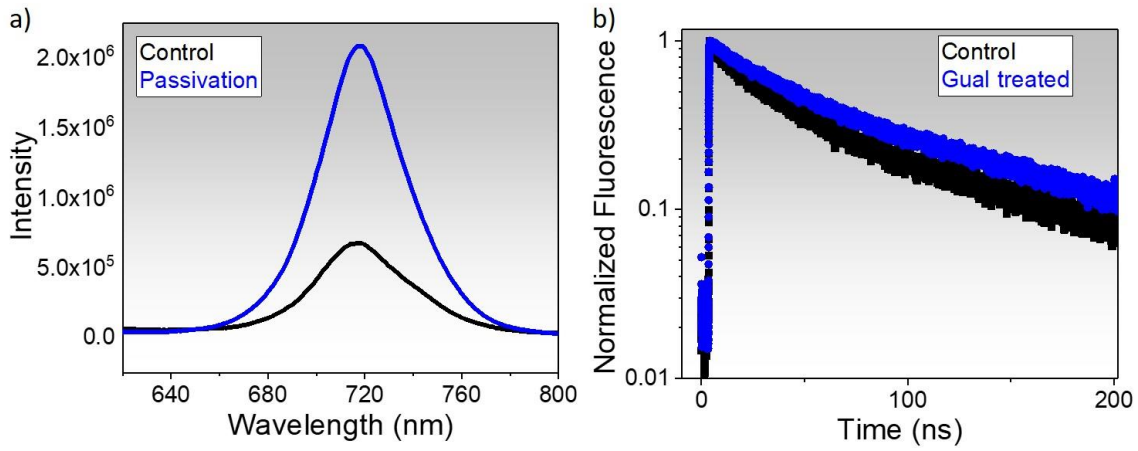

Figure S8. a) Steady-state spectra and b) time-resolved PL decays of untreated (control) and GuaI-treated 1.72 eV perovskite on glass.

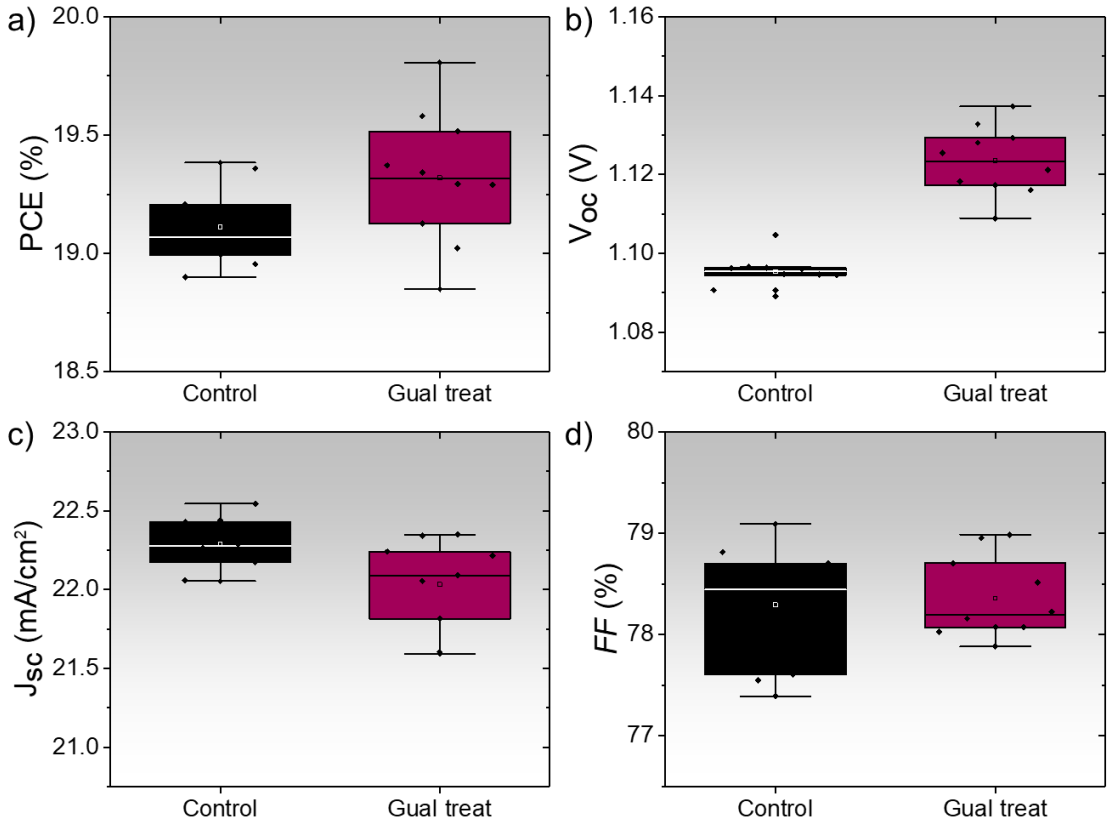

Figure S9. Photovoltaics performances of n-i-p planar untreated (control) and GuaI-treated 1.58 eV perovskite solar cells (PSCs) on glass with active area 0.16 cm^2: a) PCE, b) V_{oc} c) J_{sc} and d) Fill Factor. Statistics data over 20 PSCs for each condition.

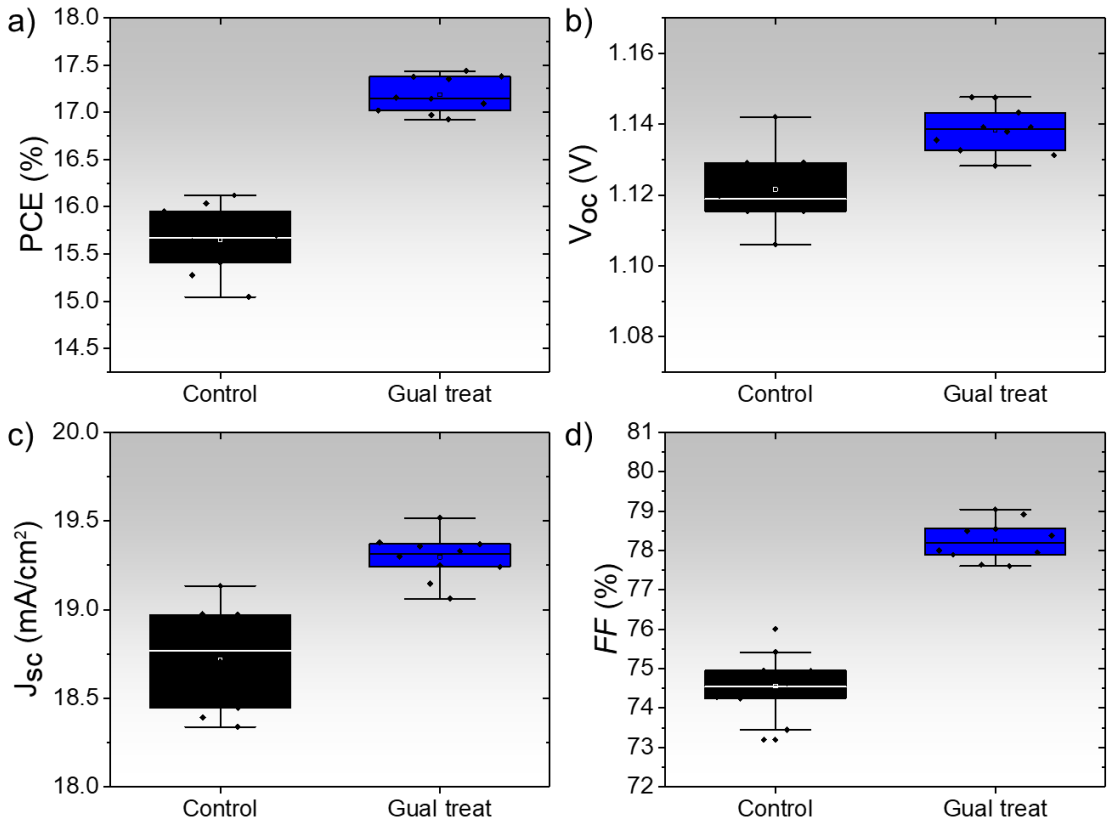

Figure S10. Photovoltaics performances of n-i-p planar untreated (control) and GuaI-treated 1.72 eV perovskite solar cells (PSCs) on glass with active area 0.16 cm^2: a) PCE, b) V_{oc} c) J_{sc} and d) Fill Factor Statistics data over 20 PSCs for each condition.

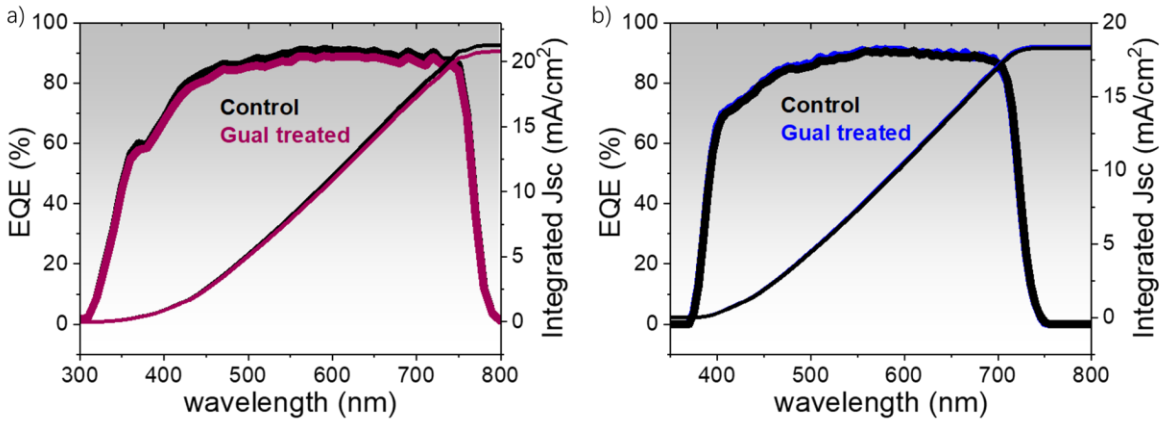

Figure S11. a) IPCE of untreated (control) and GuaI-treated 1.58 eV PSCs, b) IPCE of untreated (control) and GuaI-treated 1.72 eV PSCs.

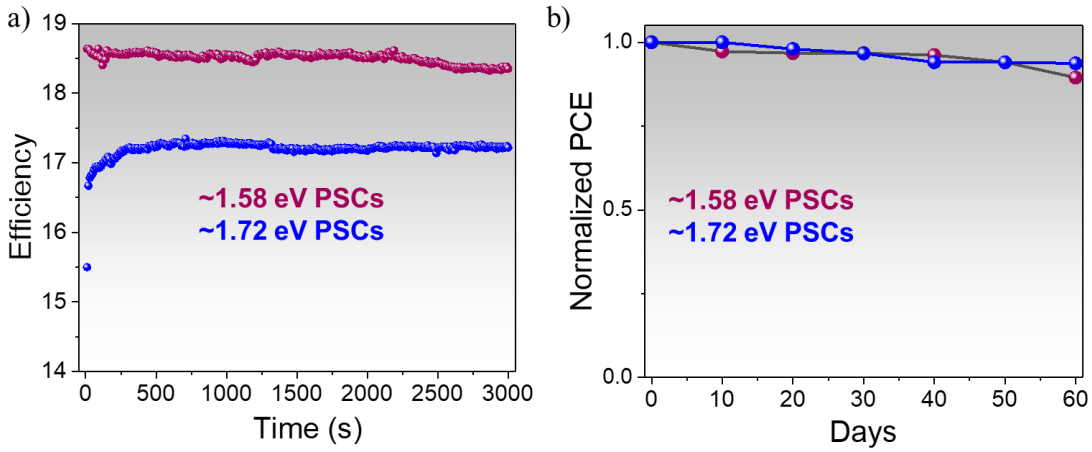

Figure S12. a) Maximum power point track over 3000 s under 1 sun condition (AM 1.5), b) shelf stability under around 35% humidity of both 1.58 and 1.72 eV PSCs.

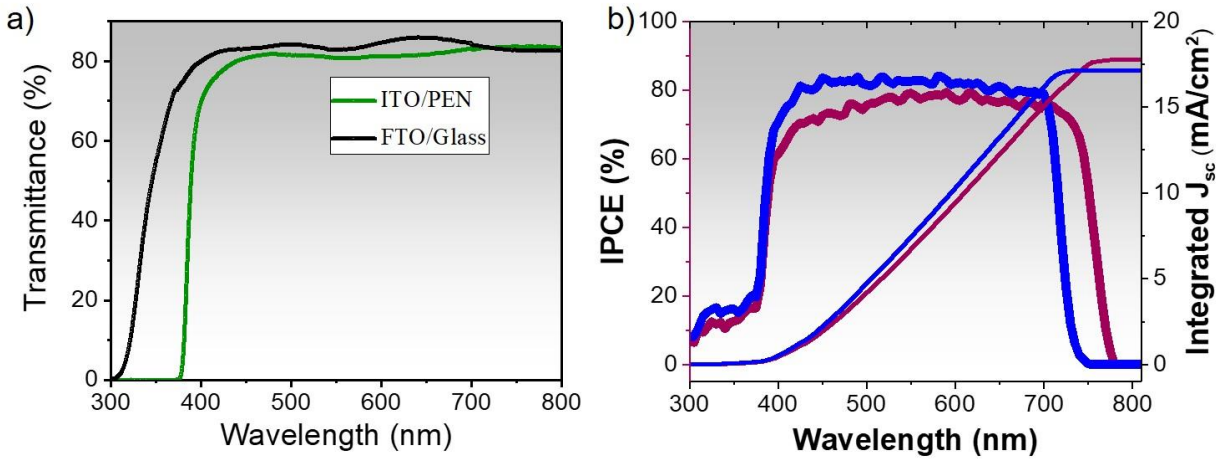

Figure S13. a) Transmittance of FTO/glass and ITO/PEN, b) IPCE of both GuaI-treated 1.58 eV and 1.72 eV PSCs on PEN substrates.

TOC GRAPHICS